JCTC Journal of Chemical Theory and Computation

Computational Studies on the Mechanisms and Dynamics of OH Reactions with $CHF_2CHFOCF_3$ and $CHF_2CH_2OCF_3$

Lei Yang, Jing-yao Liu,* and Ze-sheng Li*

Institute of Theoretical Chemistry, State Key Laboratory of Theoretical and Computational Chemistry, Jilin University, Changchun 130023, P. R. China

Received January 30, 2008

Abstract: The dual-level direct dynamics method has been employed to investigate the multichannel hydrogen abstraction reactions of $CHF_2CHFOCF_3$ + OH (R1) and $CHF_2CH_2OCF_3$ + OH (R2) theoretically. The optimized geometries and frequencies of the stationary points and the minimum energy path are calculated at the B3LYP/6-311G(d,p) level, and the energetic information is further refined by the MC-QCISD method. There are two hydrogen abstraction channels for reaction R1 and three hydrogen abstraction channels for reaction R2. And four products, $CF_2CHFOCF_3$, CHF_2CFOCF_3, $CF_2CH_2OCF_3$, and CHF_2CHOCF_3, are produced during these two reactions. The enthalpies of formation for the species involved in the two reactions ($CHF_2CHFOCF_3$, $CF_2CHFOCF_3$, CHF_2CFOCF_3, $CHF_2CH_2OCF_3$, $CF_2CH_2OCF_3$, and CHF_2CHOCF_3) are calculated via isodesmic reaction. Furthermore, the reaction mechanisms of subsequent reactions of product radicals ($CF_2CHFOCF_3$, CHF_2CFOCF_3, $CF_2CH_2OCF_3$, and CHF_2CHOCF_3) with the OH radical are studied at the same level. The rate constants of reactions R1 and R2 are evaluated by means of canonical variational transition-state theory including the small-curvature tunneling correction over a wide range of temperatures, from 250 to 1200 K. Our results show that the tunneling correction plays an important role in the rate constant calculation in the low-temperature range. Agreement between the calculated and experimental data available at 298 K is good. It is found that the fluorine substitution decreases the reactivity of the C−H bond, and as a result, reaction R2 may proceed much easier than reaction R1. The Arrhenius expressions over a wide temperature range are obtained, and the kinetic isotope effects for reactions $CHF_2CHFOCF_3/CDF_2CDFOCF_3$ + OH and $CHF_2CH_2OCF_3/CDF_2CD_2OCF_3$ + OH are estimated so as to provide theoretical estimation for future laboratory investigation.

Introduction

Since chlorofluorocarbons (CFCs) cause the depletion of the stratospheric ozone layer as well as global warming, a large number of replacement compounds such as hydrochlorofluorocarbons (HCFCs) and hydrofluorocarbons (HFCs) have been selected for industrial applications. Unfortunately, some of them have considerable global warming potentials. Furthermore, HCFCs contain Cl atoms and thus contribute to ozone depletion. Finding the suitable industrial replacement of CFCs remains a challenge, because of the complex considerations of performance, safety, and environmental properties required. Recently, hydrofluoroethers (HFEs) have been suggested as substitutes for CFCs and have been used in various industrial applications,[1,2] since they contain neither chlorine nor bromine atoms and have no ozone depletion potential (ODP).[3] Moreover, the introduction of ether linkage −O− may lead to an even greater reactivity in the troposphere, and thus HFEs are considered to be promising substitutes of CFCs. Prior to its large-scale industrial use, it is necessary to assess its environmental impact by determining its atmospheric lifetime.

* Corresponding author. Fax: +86-431-88498026. E-mail: ljy121@mail.jlu.edu.cn (J.-y. L.); zeshengli@mail.jlu.edu.cn (Z.-s. L.).

10.1021/ct800032e CCC: $40.75
Published on Web 06/14/2008

In general, the degradation of HFEs is initiated by the oxidation reaction with OH radicals in the atmosphere. Therefore, study of the reactivity of HFEs against OH radicals is important for the evaluation of their atmospheric lifetime. In the present work, our attention will focus on the reactions of molecules $CHF_2CHFOCF_3$ and $CHF_2CH_2OCF_3$ with OH radicals. As Ravishankara et al.[3] mentioned, chemical reactions involving CF_3O and CF_3OO lead to negligibly small ODPs, which means that the molecules containing CF_3 groups may be no more harmful to the stratospheric ozone layer. For the reaction of $CHF_2CHFOCF_3$ with OH, the hydrogen atom can be abstracted from α- and β-carbon atoms, so two H-abstraction channels are feasible.

$$CHF_2CHFOCF_3 + OH \rightarrow CF_2CHFOCF_3 + H_2O \quad \text{(R1a)}$$

$$CHF_2CHFOCF_3 + OH \rightarrow CHF_2CFOCF_3 + H_2O \quad \text{(R1b)}$$

Oyaro et al.[4] studied this reaction using the relative rate method, and the rate constant at 298 K was given as $(6.8 \pm 1.1) \times 10^{-15}$ cm^3 molecule^{-1} s^{-1}. However, for the reaction of $CHF_2CH_2OCF_3$ with OH, no experimental data are reported. Only Urata et al.[5] evaluated the rate constant by using the empirical estimation method to give a value of 3.27×10^{-14} cm^3 molecule^{-1} s^{-1} at 298 K. Since $CHF_2CH_2OCF_3$ has C_1 symmetry, the two hydrogen atoms in the CH_2 group are not equivalent, and as a result, three distinct channels are found, that is,

$$CHF_2CH_2OCF_3 + OH \rightarrow CF_2CH_2OCF_3 + H_2O \quad \text{(R2a)}$$

$$CHF_2CH_2OCF_3 + OH \rightarrow CF_2CHOCF_3 + H_2O \quad \text{(R2b,R2b′)}$$

To the best of our knowledge, no other experimental or theoretical study is carried out for the two reactions. Furthermore, the kinetic isotope effects (KIEs) may play an important role in investigating the kinetic nature of the reactions, but there has been no experimental determination for the two reactions. To ascertain the environmental impact of these two molecules, theoretical studies on the mechanisms of reactions $CHF_2CHFOCF_3/CHF_2CH_2OCF_3$ + OH, the temperature dependence of the rate constants, and KIEs for reactions $CHF_2CHFOCF_3/CDF_2CDFOCF_3$ + OH and $CHF_2CH_2OCF_3/CDF_2CD_2OCF_3$ + OH are very desirable.

Here, a dual-level (X//Y) direct dynamics[6–8] method is employed to study the kinetic nature of reactions R1 and R2. In this approach, dynamics calculations are based directly on the results of electronic structure calculations. As usual, X//Y refers to optimization and frequencies at a low level of theory with single-point energies from a high level of theory. The rate constants for each reaction channel are evaluated using the variational transition state theory (VTST)[9–11] with an interpolated single-point energies (ISPE) approach.[12] The centrifugal-dominant small-curvature semiclassical adiabatic ground-state tunneling (CD-SCSAG) approximation[13,14] is included. Then, the total rate constants within 250−1200 K, the product branching ratios, and KIEs are obtained. The comparison of theoretical and literature results is made.

The radicals $CF_2CHFOCF_3$, CHF_2CFOCF_3, $CF_2CH_2OCF_3$, and CHF_2CHOCF_3 are the major products produced in reactions R1 and R2, and they may further degrade through their reactions with the OH radical. However, there is no report on the properties of these radicals or their further degradation processes in the atmosphere, which are important to assess their environmental impact. Thus, the other goal of the present work is to provide deep insight into the reaction mechanism of these product radicals with OH.

$$CF_2CHFOCF_3 + OH \rightarrow \text{products} \quad \text{(R3)}$$

$$CF_2CH_2OCF_3 + OH \rightarrow \text{products} \quad \text{(R4)}$$

$$CHF_2CFOCF_3 + OH \rightarrow \text{products} \quad \text{(R5)}$$

$$CHF_2CHOCF_3 + OH \rightarrow \text{products} \quad \text{(R6)}$$

Calculation Methods

In the present study, all of the electronic structure calculations are carried out with the Gaussian 03 program.[15] The optimized geometries and harmonic vibrational frequencies of all of the stationary points (reactants, transition states, complexes, and products) involved in reactions R1–R6 are calculated by using the B3LYP method (Becke's three-parameter nonlocal-exchange functional[16] with the nonlocal correlation functional of Lee, Yang, and Parr[17]) with the 6-311G(d,p) basis set. To quantify the level of trust in the method, the geometries and harmonic vibrational frequencies of reactants, products, and transition states for reaction R1 are also performed at the MP2 level of theory (restricted or unrestricted second-order Møller−Plesset perturbation theory) with the 6-311G(d,p) basis set as well as using the BB1K method (the Becke88−Becke95 one-parameter model[18]) using the 6-31+G(d,p) basis set.[19] At the B3LYP/6-311G(d,p) and BB1K/6-31+G(d,p) levels, the minimum energy paths (MEPs) are calculated by the intrinsic reaction coordinate (IRC) theory. Also, the energy derivatives, including gradients and Hessians at geometries along the MEP, are obtained. Single-point energy calculations for the stationary points and the extra energies along the MEP are carried out using the multicoefficient correlation method based on quadratic configuration interaction with single and double excitations (MC-QCISD).[20] Then, the energy profile is refined at the MC-QCISD//B3LYP/6-311G(d,p) and MC-QCISD//BB1K/6-31+G(d,p) levels.

The initial information on the potential energy surface is put into the POLYRATE 8.4.1 program,[21] and then the dynamic calculations for reactions R1 and R2 are calculated by using VTST[9–11] with the ISPE[12] method. The ISPE method is a dual-level direct dynamics scheme, in which a few extra energies calculated at a high level of theory along the low-level MEP are used to correct the classical energetic profile of the reaction. The rate constants are calculated using canonical variational transition state theory (CVT)[22] with the CD-SCSAG approximation proposed by Truhlar and coworkers.[13,14] Most of the vibrational modes are treated as quantum-mechanical separable harmonic oscillators. The hindered-rotor approximation of Truhlar and Chuang is used

for calculating the partition functions of the lowest modes associated with the torsion. In the calculation of the electronic partition functions, the excited state of the OH radical, with a 140 cm^{-1} splitting, is included. The total rate constant of each reaction is obtained as the sum of the individual rate constant of each H-abstraction channel.

The enthalpies of formation of species are estimated by using isodesmic reactions.[23] Isodesmic reactions are those in which the number and type of bonds are conserved. Because of the electronic similarity between reactants and products, these reactions will cancel the systematic errors in the calculations and lead to accurate results. Here, we predict the enthalpies of formation for species $CHF_2CHFOCF_3$, $CF_2CHFOCF_3$, CHF_2CFOCF_3, $CHF_2CH_2OCF_3$, $CF_2CH_2OCF_3$, and CHF_2CHOCF_3 using the following isodesmic reactions:

$$CHF_2CHFOCF_3 + CH_4 \rightarrow CH_3OCH_3 + CF_3CF_3 \quad \text{(R7)}$$

$$CF_2CHFOCF_3 + CH_4 + CH_4 \rightarrow CH_3OCH_3 + CF_3 + CF_3CH_3 \quad \text{(R8)}$$

$$CHF_2CFOCF_3 + CH_4 + CH_4 \rightarrow CH_3OCH_3 + CF_3 + CF_3CH_3 \quad \text{(R9)}$$

$$CHF_2CH_2OCF_3 + CH_4 + CH_4 \rightarrow CH_3OCH_3 + CHF_2CH_3 + CHF_3 \quad \text{(R10)}$$

$$CF_2CH_2OCF_3 + CH_4 + CH_4 \rightarrow CH_3OCH_3 + CHF_2CH_3 + CF_3 \quad \text{(R11)}$$

$$CHF_2CHOCF_3 + CH_4 + CH_4 + CH_4 \rightarrow CH_3OCH_3 + CH_2F_2 + CHF_3 + CH_2CH_3 \quad \text{(R12)}$$

Results and Discussion

Electronic Structure Calculations. The optimized structural parameters of the stationary points involved in R1 and R2 calculated at the B3LYP/6-311G(d,p), BB1K/6-31+G(d,p), and MP2/6-311G(d,p) levels are displayed in Figure 1, along with the limited experimental data.[24,25] In addition, others involved in R3–R6 are given in the Supporting Information (Figure S1). As shown in Figure 1, when comparison is available, the optimized parameters at the B3LYP/6-311G(d,p), BB1K/6-31+G(d,p), and MP2/6-311G(d,p) levels are in reasonable agreement with each other. With respect to reaction R1, the reactant complexes are stabilized by the hydrogen-bond attractive interaction between O′ and H″ and between F′ and H′ (Figure 1), due to the high electronegativities of the fluorine and oxygen atoms. Also, the product complexes CP1a and CP1b with energies less than the products are located at the exits of channels R1a and R1b. For reaction R2, two reactant complexes (CR2a and CR2b) and three product complexes (CP2a, CP2b, and CP2b′) are identified at the reactant and product sides of the three channels, respectively. These indicate that each reaction channel may proceed via an indirect mechanism. With respect to the transition states TS1a, TS1b, TS2a, TS2b, and TS2b′, the breaking C−H bonds are stretched by 11.4, 12.0, 9.8, 10.5, and 11.4%, respectively, compared to the corresponding reactants, and the forming O−H bonds are longer than the equilibrium bond lengths in H_2O by 35.7, 35.1, 39.4, 34.5, and 32.7%, respectively, at the B3LYP/6-311G(d,p) level. The elongations of the forming bonds are greater than those of the breaking bonds, indicating that these transition states are all reactant-like, so H-abstraction reactions R1 and R2 may proceed via "early" transition states. The similar results can be obtained for reaction R1 at the BB1K/6-31+G(d,p) level.

The harmonic vibrational frequencies of the stationary points calculated at the B3LYP/6-311G(d,p), BB1K/6-31+G(d,p), and MP2/6-311G(d,p) levels as well as the available experimental data[24,26] are presented in Table S1 (Supporting Information). The vibrational frequencies are calculated to characterize the nature of each critical point and make zero-point energy (ZPE) correction. The number of imaginary frequencies (0 or 1) indicates whether a minimum or a transition state has been located. "Zero" imaginary frequencies correspond to a local minimum, while "one" imaginary frequency corresponds to transition structure. At the B3LYP/6-311G(d,p) level, the imaginary frequencies of TS1a, TS1b, TS2a, TS2b, and TS2b′ are 940*i*, 1009*i*, 610*i*, 790*i*, and 954*i* cm^{-1}, respectively.

Energetics. An accurate knowledge of the enthalpies of formation ($\Delta H^\circ_{f,298}$) for species is required for a thorough understanding of the kinetics and mechanisms of their reactions, particularly in atmospheric modeling. The $\Delta H^\circ_{f,298}$ values of $CHF_2CHFOCF_3$, $CF_2CHFOCF_3$, CHF_2CFOCF_3, $CHF_2CH_2OCF_3$, $CF_2CH_2OCF_3$, and CHF_2CHOCF_3 are obtained by using the calculated reaction enthalpies of the isodesmic reactions R7–R12 and the experimental $\Delta H^\circ_{f,298}$ of the other species involved in the reactions (CH_4, −17.89 kcal/mol;[27] CF_3CF_3, −321.2 kcal/mol;[27] CHF_3, −166.60 kcal/mol;[27] CF_3, −112.4 kcal/mol;[27] CH_2F_2, −107.71 kcal/mol;[27] CH_3OCH_3, −43.99 ± 0.12 kcal/mol;[28] CHF_2CH_3, −118.78 ± 0.95 kcal/mol;[29] CF_3CH_3, −178.94 kcal/mol;[30] CH_2CH_3, 28.4 ± 0.5 kcal/mol[31]). The enthalpies of formation calculated at the MC-QCISD//B3LYP/6-311G(d,p) level are −362.89 ± 0.12, −338.21 ± 0.12, −338.10 ± 0.12, −312.43 ± 1.07, −289.82 ± 1.07, and −265.36 ± 0.65 kcal/mol for $CHF_2CHFOCF_3$, $CF_2CHFOCF_3$, CHF_2CFOCF_3, $CHF_2CH_2OCF_3$, $CF_2CH_2OCF_3$, and CHF_2CHOCF_3, respectively, which are presented in Table 1. Note that the error limits are calculated by adding the maximum uncertainties of the $\Delta H^\circ_{f,298}$ values of reference species.

The reaction enthalpies (ΔH°_{298}) and potential barriers (ΔE) calculated at the MC-QCISD//B3LYP/6-311G(d,p), MC-QCISD//BB1K/6-31+G(d,p), and MC-QCISD//MP2/6-311G(d,p) levels are displayed in Table 2. As shown in Table 2, the ΔH°_{298} and ΔE values obtained at the MC-QCISD//B3LYP, MC-QCISD//BB1K, and MC-QCISD//MP2 levels show good mutual agreement. It is known that MP2 is expensive for such systems, so we employed B3LYP/6-311G(d,p) as the low level to get the rate constants of the two systems. To further verify the reliability of B3LYP, we also performed the dynamic calculations for reaction R1 at the MC-QCISD//BB1K/6-31+G(d,p) level.

Schematic potential energy surfaces obtained at the MC-QCISD//B3LYP/6-311G(d,p) level for reactions $CHF_2CHFOCF_3$ + OH (R1) and $CHF_2CH_2OCF_3$ + OH (R2) are

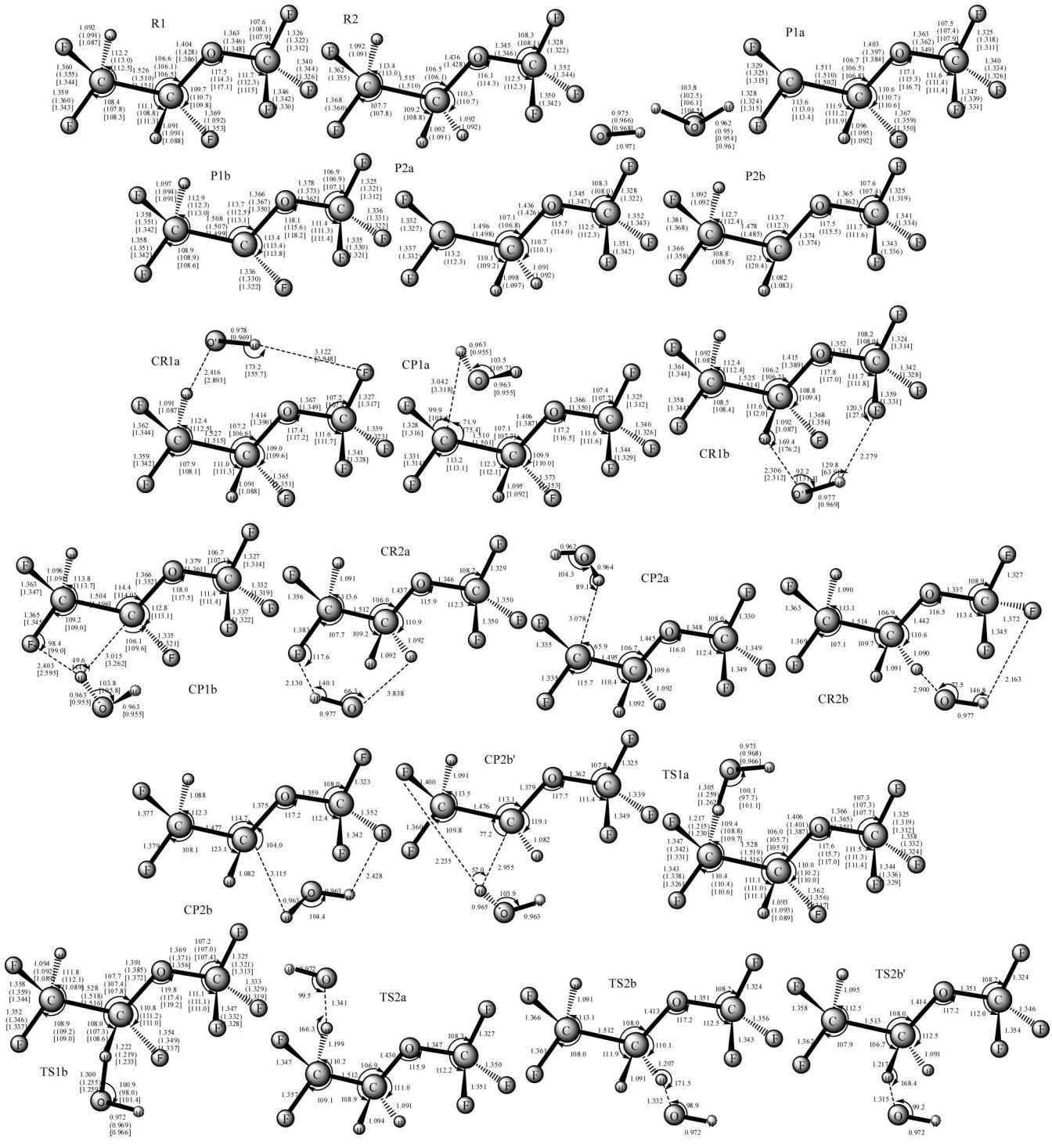

Figure 1. Optimized geometries of reactants, products, complexes, and transition states at the B3LYP/6-311G(d,p), MP2/6-311G(d,p) (in parentheses), and BB1K/6-31+G(d,p) (in square brackets) levels of reactions $CHF_2CH_2OCF_3/CHF_2CHFOCF_3$ + OH. The numbers in curly brackets are the experimental values.[24,25] Bond lengths are in angstroms, and angles are in degrees.

plotted in Figure 2a and b. The energy of reactant is set to zero for reference. Seen from Figure 2a, we can find that two hydrogen-bond complexes, CR1a (−2.54 kcal/mol) and CR1b (−0.57 kcal/mol), are located at the reactant side of channels R1a and R1b, respectively. And two complexes, CP1a and CP1b, with the energies being 0.52 and 0.57 kcal/mol lower than the products, are located at the product sides of R1a and R1b, respectively. The barrier height of channel R1a is 4.61 kcal/mol, which is only about 0.8 kcal/mol lower than that of channel R1b. Furthermore, channels R1a and R1b are exothermic at about −16.81 and −16.77 kcal/mol, which is almost the same. Thus, H abstractions from $-CHF_2$ and $-CH_2-$ groups may be kinetically and thermodynamically competitive channels. Furthermore, the relative energies of the transition states, complexes, and products obtained at the MC-QCISD//BB1K level are also displayed in Figure

Table 1. Enthalpies of Formation (kcal/mol) of the Species $CHF_2CHFOCF_3$, $CF_2CHFOCF_3$, CHF_2CFOCF_3, $CHF_2CH_2OCF_3$, $CF_2CH_2OCF_3$, and CHF_2CHOCF_3 Calculated at the MC-QCISD//B3LYP/6-311G(d,p) Level

species	$\Delta H^{\circ}_{f,298}$	species	$\Delta H^{\circ}_{f,298}$
$CHF_2CHFOCF_3$	-362.89 ± 0.12	$CHF_2CH_2OCF_3$	-312.43 ± 1.07
$CF_2CHFOCF_3$	-338.21 ± 0.12	$CF_2CH_2OCF_3$	-289.82 ± 1.07
CHF_2CFOCF_3	-338.10 ± 0.12	CHF_2CHOCF_3	-265.36 ± 0.62

2a. It is seen that the barrier heights obtained at the MC-QCISD//BB1K level are in good agreement with those obtained at the MC-QCISD//B3LYP level. At the B3LYP/6-311G(d,p) level, two hydrogen-bond complexes (CR2a and CR2b) are located at the reactant side of the channels (R2a and R2b) of reaction R2; the stabilization energies are −1.45 and −1.91 kcal/mol for CR2a and CR2b, respectively. Also, three complexes, CP2a, CP2b, and CP2b′, are located at the exits of channels R2a, R2b, and R2b′ with the energies lower than the corresponding products. With respect to the transition states of R2, the relative energy of TS2b, 4.10 kcal/mol, is the lowest one, indicating that OH attack on the H atoms in the $-CH_2-$ group is most favored kinetically. In addition, TS2b′ (H′ in the $-CH_2-$ group is abstracted by OH) lies about 0.8 kcal/mol higher than TS2b. By analysis, we find that, for channel R2b, the abstracted hydrogen (H) lies between H and F, whereas for channel R2b′, the abstracted hydrogen (H′) lies between F and F, so the steric hindrance for channel R2b′ is a little larger than the one for channel R2b, which leads to the higher potential energy barrier of R2b. Although the barrier height of channel R2a is about 0.4 kcal/mol lower than that of R2b′, the latter is more exothermic than the former by about 2.6 kcal/mol. So, channels R2a and R2b′ are expected to be competitive, while channel R2b is the dominant route kinetically and thermodynamically. This view is further supported in the following rate constant study. In addition, the energies of transition state TS1b (5.43 kcal/mol, relative to the reactants) is higher than those of TS2b (4.10 kcal/mol) and TS2b′ (4.93 kcal/mol) at the MC-QCISD//B3LYP/6-311G(d,p) level, indicating that the substitution of H by F decreases the reactivity of the C−H bond toward hydrogen abstraction. A similar conclusion can be obtained from the reactions OH with CH_3OCH_3 and CF_3OCH_3.[32]

Now, our focus will be fixed on the subsequent reactions of product radicals with OH: $CF_2CHFOCF_3$ + OH (R3), $CF_2CH_2OCF_3$ + OH (R4), CHF_2CFOCF_3 + OH (R5), and CHF_2CHOCF_3 + OH (R6). The potential energy surfaces (PESs) of these reactions obtained at the B3LYP/6-311G(d,p) level are shown in Figure 3a and b. From Figure 3a and b, we can find that all of these reactions take the addition−elimination mechanisms. Without any association barriers, the OH radical initially attacks the product radicals on the free radical site via electrostatic interaction between the reactant species. These are barrierless association processes, and four intermediates, M1, M2, M3, and M4, are produced with the energies 111.36, 109.33, 106.93, and 99.77 kcal/mol, respectively, lower than the reactants. Starting from M1, it can take the concerted 1,3-H-shift and C−H-bond-rupture processes to form product complex CP1 (−75.13 kcal/mol). Subsequently, CP1 dissociates to the final products CF_2CFOCF_3 and H_2O, that is,

$$CF_2CHFOCF_3 + OH \rightarrow C(OH)F_2CHFOCF_3\ (M1) \rightarrow CP1 \rightarrow CF_2CFOCF_3 + H_2O \quad (R3)$$

A similar case can be found in reactions $CF_2CH_2OCF_3$ + OH (R4) and CHF_2CFOCF_3 + OH (R5). However, the case is different for reaction CHF_2CHOCF_3 + OH (R6). The intermediate M4 has two H atoms which are not equivalent. With the large amount of heat released from the addition processes, M4 can take a concerted 1,3-H shift and cleavage of a neighbor C−H bond via transition state TS4, forming CF_2CHOCF_3 and H_2O, which is similar to the situation discussed above. Also, M4 can take a concerted 1,2-H shift and adjacent C−H cleavage to form CP5 via transition state TS5 and then produce products CHF_2COCF_3 and H_2O. These reactions can be summarized as follows:

$$CF_2CH_2OCF_3 + OH \rightarrow C(OH)F_2CH_2OCF_3\ (M2) \rightarrow CP2 \rightarrow CF_2CHOCF_3 + H_2O \quad (R4)$$

$$CHF_2CFOCF_3 + OH \rightarrow CHF_2C(OH)FOCF_3\ (M3) \rightarrow CP3 \rightarrow CF_2CFOCF_3 + H_2O \quad (R5)$$

$$CHF_2CHOCF_3 + OH \rightarrow CHF_2CH(OH)OCF_3\ (M4) \rightarrow CP4 \rightarrow CF_2CHOCF_3 + H_2O \quad (R6a)$$

$$CHF_2CHOCF_3 + OH \rightarrow CHF_2CH(OH)OCF_3\ (M4) \rightarrow CP5 \rightarrow CHF_2COCF_3 + H_2O \quad (R6b)$$

From Figure 3a and b, we can see that all of the transition states and products lie below the respective reactants, which means that the addition−elimination processes are all thermodynamically and kinetically accessible, and the products CF_2CFOCF_3, CF_2CHOCF_3, and CHF_2COCF_3 may be easily produced during these processes. So, these products may be expected to be observed experimentally. We hope that the present theoretical prediction may assist in future laboratory investigations.

Dynamic Calculations. For the H-abstraction reactions R1 and R2, direct dynamic calculations are performed on the basis of the electronic structure information above. The reactant and product complexes for the reaction channel (if it exists) are taken into account in the dynamic calculations performed by the Polyrate program. Similar cases have been discussed by Galano et al.[33] The MEPs of reactions R1 and R2 are calculated by IRC theory at the B3LYP/6-311G(d,p) level, and the potential energy profile is further improved with the ISPE method at the MC-QCISD//B3LYP level. As pointed out by Truhlar et al.,[34] four single-point calculations are important to correct the lower-level reaction path for the ISPE method: two points are close to the 300 K turning points and are useful primarily to estimate the width of the barrier; two other points are close to the lower-level saddle point and are useful primarily to locate the dual-level saddle point. So the single-point energies evaluated at four extra points (denoted as VTST−ISPE-4) are used for the spline fit. For the purpose of comparison, the dynamics calculations of reaction R1 are also carried out with the VTST method at the MC-QCISD//BB1K level.

Table 2. The Enthalpies (ΔH°_{298}) and Potential Barriers (ΔE) (kcal/mol) with ZPE Correction at the MC-QCISD//B3LYP, MC-QCISD//BB1K, and MC-QCISD//MP2 Levels

levels	MC-QCISD//B3LYP		MC-QCISD//BB1K		MC-QCISD//MP2	
	ΔH°_{298}	ΔE	ΔH°_{298}	ΔE	ΔH°_{298}	ΔE
$CHF_2CHFOCF_3 + OH \rightarrow CF_2CHFOCF_3 + H_2O$ (R1a)	−16.51	4.61	−16.33	4.32	−16.45	4.67
$CHF_2CHFOCF_3 + OH \rightarrow CHF_2CFOCF_3 + H_2O$ (R1b)	−16.39	5.43	−16.18	5.36	−16.19	5.36
$CHF_2CH_2OCF_3 + OH \rightarrow CF_2CH_2OCF_3 + H_2O$ (R2a)	−17.55	4.46			−17.55	
$CHF_2CH_2OCF_3 + OH \rightarrow CHF_2CHOCF_3 + H_2O$ (R2b)	−20.07	4.10			−19.95	
$CHF_2CH_2OCF_3 + OH \rightarrow CHF_2CHOCF_3 + H_2O$ (R2b′)	−20.07	4.93			−19.95	

Figure 4 shows the plot of the classical potential energy curve (V_{MEP}), ground-state vibrationally adiabatic energy curve (V_a^G), and zero-point energy curve (ZPE) as functions of s (amu)$^{1/2}$·bohr at the MC-QCISD//B3LYP level for channel R1a, where $V_a^G = V_{MEP} + ZPE$. Due to the similarity, the plots for R1b, R2a, R2b, and R2b′ are depicted in Figure S4 (Supporting Information). From Figure 4, we can find that the ZPE is practically constant as s varies, with only a gentle drop near the saddle point. The V_{MEP} and V_a^G curves are similar in shape, and the maxima are also located at the same position, implying that the variational effect will be small. The following study will further support this view.

The rate constants of each reaction channel are calculated by using TST, CVT, and CVT with small-curvature tunneling (SCT) correction over the temperature range 250−1200 K at the MC-QCISD//BLYP/6-311G(d,p) level. The plots of

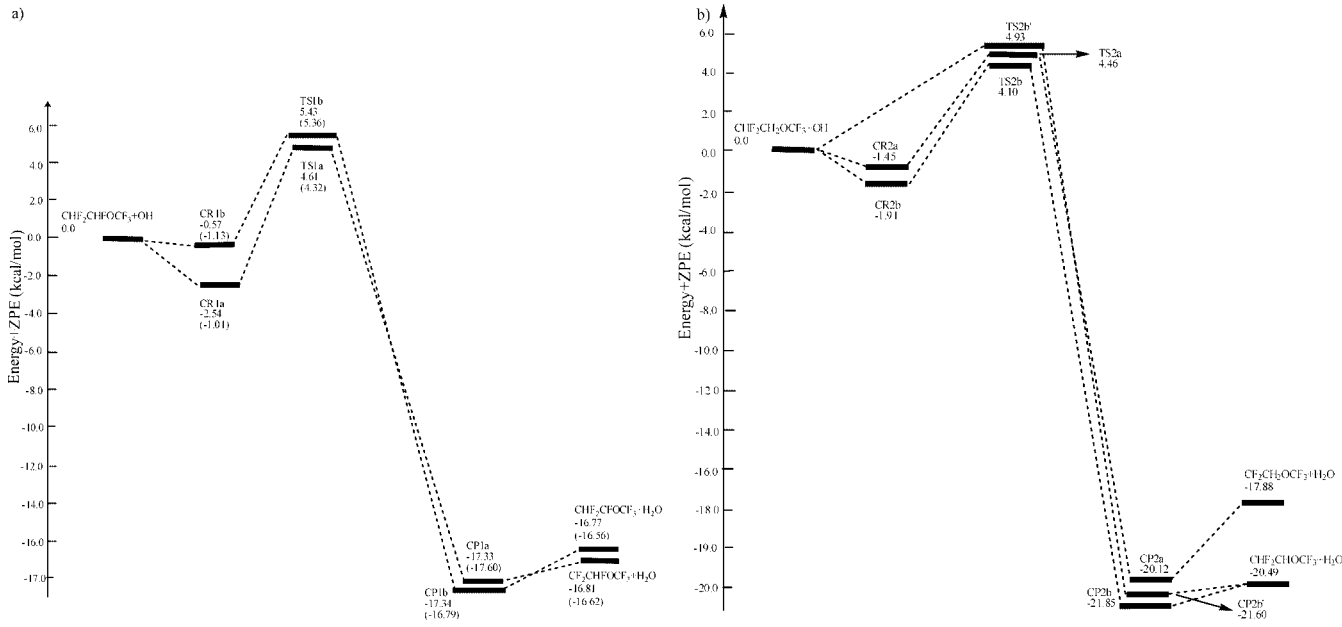

Figure 2. (a) Schematic potential energy surfaces for reaction $CHF_2CHFOCF_3 + OH$. Relative energies (in kcal/mol) are calculated at the MC-QCISD//B3LYP+ZPE and MC-QCISD//BB1K+ZPE levels. (b) Schematic potential energy surfaces for reaction $CHF_2CH_2OCF_3 + OH$. Relative energies (in kcal/mol) are calculated at the MC-QCISD//B3LYP+ZPE level.

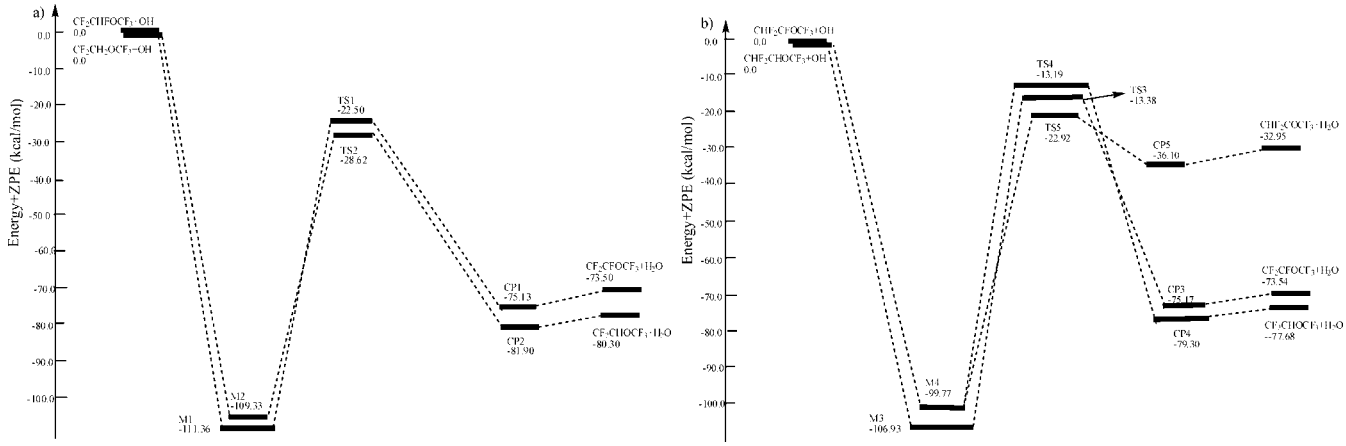

Figure 3. Schematic potential energy surfaces for reactions $CF_2CHFOCF_3/CF_2CH_2OCF_3 + OH$. Relative energies (in kcal/mol) are calculated at the MC-QCISD//B3LYP/6-311G(d, p)+ZPE level. (b) Same as part a except for reactions $CHF_2CFOCF_3/CHF_2CHOCF_3 + OH$.

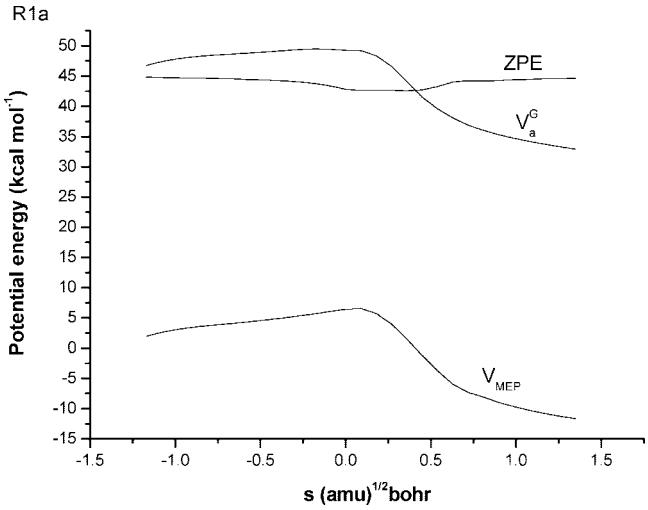

Figure 4. Classical potential energy curve (V_{MEP}), ground-state vibrationally adiabatic energy curve (V_a^G), and zero-point energy curve (ZPE) as functions of s (amu)$^{1/2}$ bohr at the MC-QCISD//B3LYP/6-311G(d,p) level for channel $CHF_2CHFOCF_3 + OH \rightarrow CF_2CHFOCF_3 + H_2O$ (R1a).

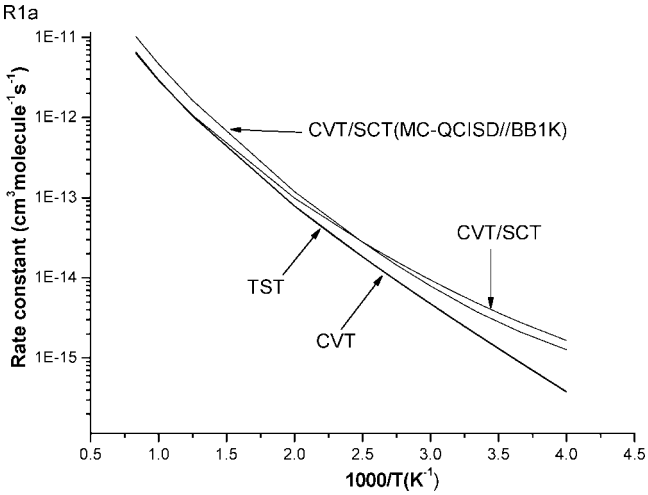

Figure 5. The TST, CVT, and CVT/SCT rate constants calculated at the MC-QCISD//B3LYP level and the CVT/SCT rate constants calculated at the MC-QCISD//BB1K level as a function of 10^3/T for the reaction channel R1a.

TST, CVT, and CVT/SCT rate constants of channel R1a as functions of the reciprocal of the temperature are present in Figure 5, and the corresponding plots of R1b, R2a, R2b, and R2b′ are shown in Figure S5 (Supporting Information). Also, the calculated CVT/SCT rate constants at the MC-QCISD//BB1K/6-31+G(d,p) level for channels R1a (k'_{1a}) and R2a (k'_{1b}) are displayed in Figures 5 and Figure S5 (Supporting Information), respectively. Seen from the figures, the calculated CVT/SCT rate constants at the MC-QCISD//B3LYP level agree well with those obtained at the MC-QCISD//BB1K level. At the MC-QCISD//B3LYP level, the TST and CVT rate constants for H abstraction from $-CHF_2$ are very close over the whole temperature range, which indicates that the variational effect is small. These results are in accord with the above analysis. Moreover, by contrasting the CVT and CVT/SCT rate constants, it is found that SCT correction plays an important role for each channel at the lower temperatures. For example, the ratios of $k_{CVT/SCT}/k_{CVT}$ at 250 K are 4.4, 1.1, 4.6, 9.5, and 11.4 for R1a, R1b, R2a, R2b, and R2b′, respectively.

The total rate constants of R1 and R2 are obtained as the sum of the individual rate constants associated with the corresponding channels. Figure 6 presents the individual CVT/SCT rate constants of each reaction channel of R1 and R2 (k_{1a}, k_{1b}, k_{2a}, k_{2b}, and $k_{2b'}$) and the total rate constants k_1 and k_2 ($k_1 = k_{1a} + k_{1b}$ and $k_2 = k_{2a} + k_{2b} + k_{2b'}$) obtained at the MC-QCISD//B3LYP level, along with the available literature values.[4,5] Also, the total rate constants of channel R1 calculated at the MC-QCISD//BB1K level ($k'_1 = k'_{1a} + k'_{1b}$) are plotted in Figure 6 for comparison. In addition, the temperature dependence of the k_{1a}/k_1, k_{1b}/k_1, k_{2a}/k_2, k_{2b}/k_2, and $k_{2b'}/k_2$ branching ratios is plotted in Figure 7. For reaction R1, H abstraction from the $-CHF_2$ group (R1a) is a more competitive channel over the whole temperature range, whereas the contribution of channel R1b should be considered at the lower temperature range. For example, k_{1a}/k_1 branching ratios are 71.2, 88.7, and 96.1% at 298, 500, and 1200 K, respectively. From Figure 6, we can see that the total rate constants calculated at the two levels show good agreement in the whole temperature range, within a factor of 0.6−1.2. The values of k_1 and k'_1 are 6.64×10^{-15} and 5.33×10^{-15} cm^3 molecule^{-1} s^{-1} at 298 K, respectively, which are consistent with the only experimental value [$(6.80 \pm 1.1) \times 10^{-15}$ cm^3 molecule^{-1} s^{-1}] obtained by Oyaro et al.[4] The good agreements between theoretical and experimental values and between the results at the two levels imply that the B3LYP method is reliable in the location of the transition state and the reaction path for such systems. So, for reaction R2, the dynamic calculations are just performed at the MC-QCISD//B3LYP level. For reaction R2, seen in Figure 7, the dominant reaction channel is channel R2b, that is, H abstraction from the $-CH_2-$ group, leading to the product CHF_2CHOCF_3, and the channels R2a and R2b′ are competitive channels. The k_{2a}/k_2, k_{2b}/k_2, and $k_{2b'}/k_2$ branching ratios are 16.4, 73.4, and 10.2% at 298 K and 28.3, 42.0, and 29.7% at 1200 K. Thus, all of these channels (R2a, R2b, and R2b′) should be taken into account over the whole temperature range. Our calculated rate constant at 298 K (2.74×10^{-14} cm^3 molecule^{-1} s^{-1}) is slightly lower than the available literature value, 3.27×10^{-14} cm^3 molecule^{-1} s^{-1}, estimated by using the empirical estimation method.[5] In addition, the rate constant of reaction R2 (k_2) is about 1 order of magnitude larger than that of reaction R1 (k_1); that is to say, reaction R2 may proceed much easier than reaction R1, and the fluorine substitution decreases the reactivity of the C−H bond. This is because F is strongly electron-withdrawing; the electron density on the carbon atom of $-CHF$ is more reduced in $CHF_2CHFOCF_3$ than that of $-CH_2-$ in $CHF_2CH_2OCF_3$. Consequently, the smaller rate constants are found for reaction R1.

The rate constants exhibit strong non-Arrhenius behavior in the temperature range of 250−1200 K. Since there is little experimental data for these two reactions, to provide useful guides for future experimental study, the three-parameter fits based on the CVT/SCT rate constants within 250−1200 K give the expressions as follows (in units of cm^3 molecule^{-1} s^{-1}): $k_1 = [2.49 \times 10^{-24}]T^{4.10} \exp(-488/T)$, $k_2 = [4.26 \times 10^{-23}]T^{3.80} \exp(-404/T)$.

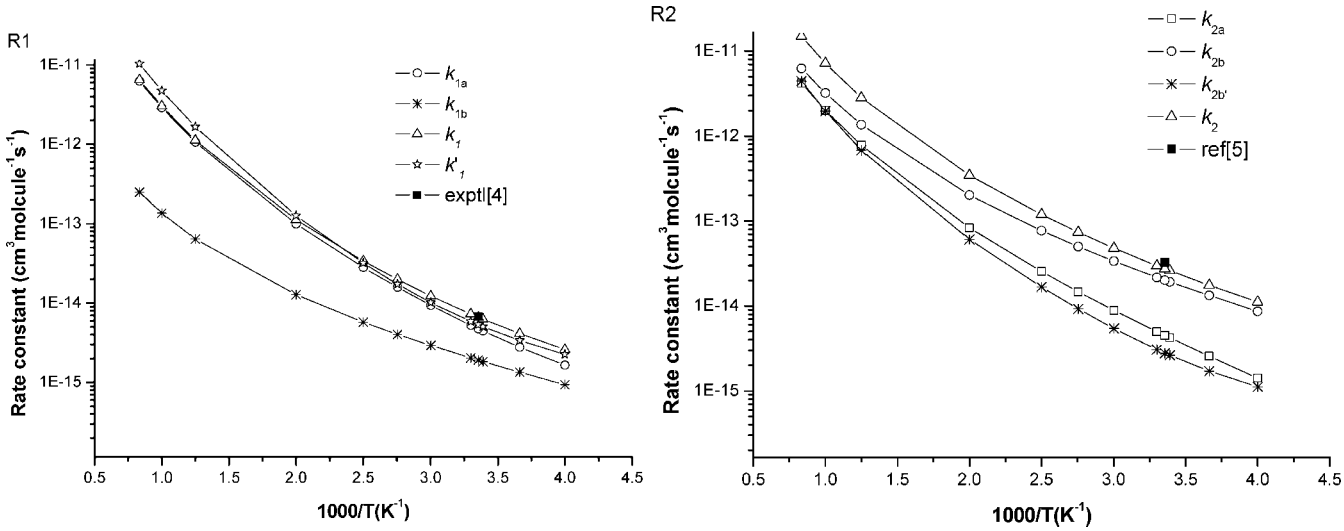

Figure 6. The rate constants k_{1a} and k_{1b} for the reaction channels of $CHF_2CHFOCF_3$ + OH and k_{2a}, k_{2b}, and $k_{2b'}$ for $CHF_2CH_2OCF_3$ + OH; the total rate constants k_1 ($k_1 = k_{1a} + k_{1b}$) and k_2 ($k_2 = k_{2a} + k_{2b} + k_{2b'}$) calculated at the MC-QCISD//B3LYP/6-311G(d, p) level; and the total rate constants k'_1 ($k'_1 = k'_{1a} + k'_{1b}$) calculated at the MC-QCISD//BB1K/6-31+G(d,p) level along with the literature values[4,5] as a function of 10^3/T.

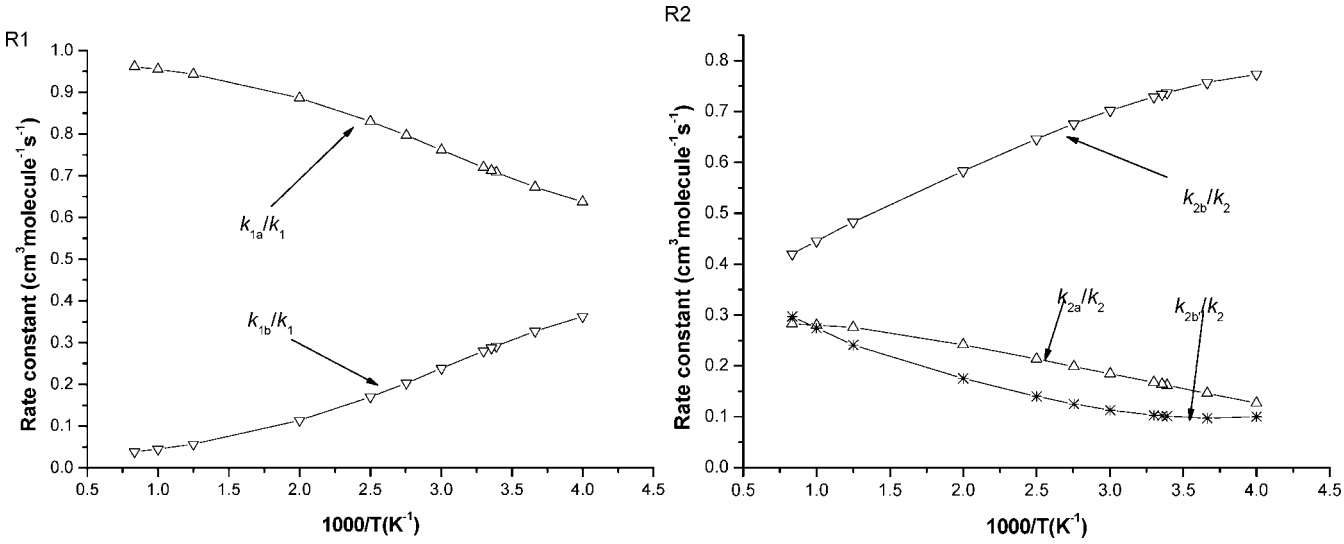

Figure 7. Calculated branching ratio for reactions $CHF_2CHFOCF_3$ + OH and $CHF_2CH_2OCF_3$ + OH as a function of 10^3/T at the MC-QCISD//B3LYP/6-311G(d, p) level.

Furthermore, the kinetic isotope effects for the reactions $CHF_2CHFOCF_3$ + OH (R1)/$CDF_2CDFOCF_3$ + OH (R1*) and $CHF_2CH_2OCF_3$ + OH (R2)/$CDF_2CD_2OCF_3$ + OH (R2*) are calculated over the whole temperature range. The calculated KIEs for the total reactions R1 (k_1/k_1*) and R2 (k_2/k_2*) are shown in Figure 8, and the KIEs for individual channels R1a, R1b, R2a, R2b, and R2b′ are displayed in the Supporting Information (Figure S8). As shown in Figure 8, the two reactions present normal KIEs, that is, greater than 1. The KIE values are 12.2 and 2.0 at 298 K for reactions R1 and R2, respectively, and the KIEs decrease with the temperature increase. Since there is no experimental value to make a comparison, we hope the present predictions for KIEs may be helpful for future experimental investigations.

Conclusions

In this paper, the dual-level direct dynamic method is employed to investigate theoretically the hydrogen abstraction reaction systems $CHF_2CHFOCF_3$ + OH (R1) and $CHF_2CH_2OCF_3$ + OH (R2). The PES information is obtained at the B3LYP/6-311G(d,p) level, and the higher-level energies for the stationary points and extra points along the minimum energy path are refined at the MC-QCISD theory. Two and three hydrogen abstraction channels are found for reactions R1 and R2, respectively, and four products, $CF_2CHF_2OCF_3$, $CHF_2CF_2OCF_3$, $CF_2CH_2OCF_3$, and CHF_2CHOCF_3, are produced. Using group balance isodesmic reactions as working reactions, the $\Delta H^{\circ}_{f,298}$ values are -362.89 ± 0.12, -338.21 ± 0.12, -338.10 ± 0.12, -312.43 ± 1.07, -289.82 ± 1.07, and -265.36 ± 0.65 kcal/mol for $CHF_2CHFOCF_3$, $CF_2CHFOCF_3$, CHF_2CFOCF_3, $CHF_2CH_2OCF_3$, $CF_2CH_2OCF_3$, and CHF_2CHOCF_3, respectively, at the MC-QCISD//B3LYP/6-311G(d,p) level. Furthermore, the subsequent reaction mechanisms of the reactions of the above four product radicals with the OH radical are

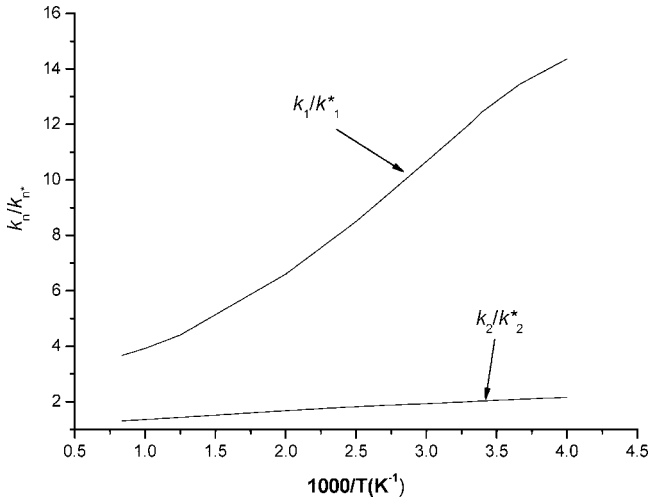

Figure 8. Plot of the calculated ratios k_1/k^*_1 and k_2/k^*_2 versus 1000/T at the temperature range 250−1200 K.

investigated theoretically at the same level in this article. We found that all of these reactions take the addition−elimination mechanisms. These processes are all thermodynamically and kinetically accessible, and the products CF_2CFOCF_3, CF_2CHOCF_3, CHF_2COCF_3, and H_2O are expected to be observed. The rate constants of the H-abstraction reaction channels are calculated by using CVT with the SCT correction. For each H-abstraction reaction channel, the variational effect is small over the whole temperature region, and the SCT correction plays an important role in the rate constant calculation in the lower-temperature range. For reaction R1, H abstraction from the $-CHF_2$ group (R1a) is the more competitive channel over the whole temperature range, whereas the contribution of channel R1b should be considered at the lower temperatures. For reaction R2, the preferred reaction channel is channel R2b. However, the contribution of channels R2a and R2b′ should be also taken into account over the whole temperature range. In addition, the rate constant of reaction R2 (k_2) is about 1 order of magnitude larger than that of reaction R1 (k_1). To provide good estimation for future laboratory investigations, the fitted three-parameter expressions within 250−1200 K for these two reactions are given, $k_1 = [2.49 \times 10^{-24}]T^{4.10} \exp(-488/T)$, $k_2 = [4.26 \times 10^{-23}]T^{3.80} \exp(-404/T)$ cm^3 molecule^{-1} s^{-1}.

Acknowledgment. We thank Professor Donald G. Truhlar for providing the POLYRATE 8.4.1 program. This work is supported by the National Natural Science Foundation of China (Grants 20333050, 20073014, and 20303007), Doctor Foundation by the Ministry of Education Foundation for University Key Teacher by the Ministry of Education, Key Subject of Science and Technology by the Ministry of Education of China, and the Innovation Foundation by Jilin University.

Supporting Information Available: Calculated frequencies, potential energy curves, computed rate constant curves, and a plot of calculated ratios. This material is available free of charge via the Internet at http://pubs.acs.org.

References

(1) Sekiya, A.; Misaki, S. *J. Fluorine Chem.* **2000**, *101*, 215.

(2) Sekiya, A.; Misaki, S. *CHEMTECH* **1996**, *26*, 44.

(3) Ravishankara, R. A.; Turnipseed, A. A.; Jensen, N. R.; Barone, S.; Mills, M.; Howark, C. J.; Solomon, S. *Science* **1994**, *263*, 71.

(4) Oyaro, N.; Sellevag, S. R.; Nielsen, C. J. *J. Phys. Chem. A* **2005**, *109*, 337.

(5) Urata, S.; Takada, A.; Uchimaru, T.; Chandra, A. K. *Chem. Phys. Lett.* **2003**, *368*, 215.

(6) Truhlar, D. G. In *The Reaction Path in Chemistry: Current Approaches and Perspectives*; Heidrich, D. , Ed.; Kluwer: Dordrecht, The Netherlands, 1995; pp 229.

(7) Truhlar, D. G.; Garrett, B. C.; Klippenstein, S. J. *J. Phys. Chem.* **1996**, *100*, 12771.

(8) Hu, W. P.; Truhlar, D. G. *J. Am. Chem. Soc.* **1996**, *118*, 860.

(9) Truhlar, D. G.; Garrett, B. C. *Acc. Chem. Res.* **1980**, *13*, 440.

(10) Truhlar, D. G.; Isaacson, A. D.; Garrett, B. C. In *The Theory of Chemical Reaction Dynamics*; Baer, M., Ed.; CRC Press: Boca Raton, FL, 1985; pp 65.

(11) Truhlar, D. G.; Garrett, B. C. *Annu. Rev. Phys. Chem.* **1984**, *35*, 159.

(12) Chuang, Y. Y.; Corchado, J. C.; Truhlar, D. G. *J. Phys. Chem. A* **1999**, *103*, 1140.

(13) Lu, D. H.; Truong, T. N.; Melissas, V. S.; Lynch, G. C.; liu, Y. P.; Garrett, B. C.; Steckler, R.; Issacson, A. D.; Rai, S. N.; Hancock, G. C.; Lauderdale, J. G.; Joseph, T.; Truhlar, D. G. *Comput. Phys. Commun.* **1992**, *71*, 235.

(14) Liu, Y.-P.; Lynch, G. C.; Truong, T. N.; Lu, D.-H.; Truhlar, D. G.; Garrett, B. C. *J. Am. Chem. Soc.* **1993**, *115*, 2408.

(15) Frisch, M. J.; Truck, G. W.; Schlegel, H. B.; Scuseria, G. E.; Robb, M. A.; Cheeseman, J. R.; Zakrzewski, V. G.; Montgomery, J. A., Jr.; Stratmann, R. E.; Burant, J. C.; Dapprich, S.; Millam, J. M.; Daniels, A. D.; Kudin, K. N.; Strain, M. C.; Farkas, O.; Tomasi, J.; Barone, V.; Cossi, M.; Cammi, R.; Mennucci, B.; Pomelli, C.; Adamo, C.; Clifford, S.; Ochterski, J.; Petersson, G. A.; Ayala, P. Y.; Cui, Q.; Morokuma, K.; Malick, D. K. ; Rabuck, A. D. ; Raghavachari, K.; Foresman, J. B.; Cioslowski, J.; Ortiz, J. V.; Boboul, A. G.; Stefnov, B. B.; Liu, G.; Liaschenko, A.; Piskorz, P.; Komaromi, L.; Gomperts, R.; Martin, R. L.; Fox, D. J.; Keith, T.; AlLaham, M. A.; Peng, C. Y.; Nanayakkara, A.; Gonzalez, C.; Challacombe, M.; Gill, P. M. W.; Johnson, B.; Chen, W.; Wong, M. W.; Andres, J. L.; Gonzalez, C.; Head-Gordon, M.; Replogle, E. S.; Pople, J. A. *GAUSSIAN 03*, revision A.1 ed.; Guassian, Inc.: Pittsburgh, PA, 2003.

(16) Becke, A. D. *J. Chem. Phys.* **1993**, *98*, 1372.

(17) Lee, C.; Yang, W.; Parr, R. G. *Phys. Rev. B: Condens. Matter Mater. Phys.* **1988**, *37*, 785.

(18) Zhao, Y.; Lynch, B. J.; Truhlar, D. G. *J. Phys. Chem. A* **2004**, *108*, 2715.

(19) Lynch, B. J.; Zhao, Y.; Truhlar, D. G. *J. Phys. Chem. A* **2003**, *107*, 1384.

(20) Fast, P. L.; Truhlar, D. G. *J. Phys. Chem. A* **2000**, *104*, 6111.

(21) Chuang, Y.-Y.; Corchado, J. C.; Fast, P. L.; Villa, J.; Hu, W.-P.; Liu, Y.-P.; Lynch, G. C.; Jackels, C. F.; Nguyen, K. A.; Gu, M. Z.; Rossi, I.; Coitino, E. L.; Clayton, S.; Melissas, V. S.; Lynch, B. J.; Steckler, R.; Garrett, B. C.; Isaacson,

A. D.; Truhlar, D. G.; *Polyrate*, version 8.4.1 ed.; University of Minnnesota: Minneapolis, MN, 2000.

(22) Garrett, B. C.; Truhlar, D. G. *J. Chem. Phys.* **1979**, *70*, 1593.

(23) Good, D. A.; Francisco, J. S. *J. Phys. Chem. A* **1998**, *102*, 7143.

(24) Huber, K. P.; Herzberg, G. In *Molecular Spectra and Molecular Structure. IV. Constants of Diatomic Molecules*; Van Nostrand Reinhold Co.: New York, 1979.

(25) Hoy, A. R.; Bunker, P. R. *J. Mol. Struct.* **1979**, *74*, 1.

(26) Shimanouchi, T. *Tables of Molecular Vibrational Frequencies, Consolidated 1, NSRDS NBS-39*; U.S. Department of Commerce: Washington, DC.

(27) Chase, M. W., Jr *J. Phys. Chem. Ref. Data, Monograph* **1998**, *9*, 1.

(28) Pilcher, G.; Pell, A. S.; Coleman, D. J. *Trans. Faraday Soc.* **1964**, *60*, 499.

(29) Kolesov, V. P.; Shtekher, S. N.; Martynov, A. M.; Skuratov, S. M. *Russ. J. Phys. Chem. (Engl. Transl.)* **1968**, *42*, 975.

(30) Wu, E.; Rodgers, A. S. *J. Phys. Chem.* **1974**, *78*, 2315.

(31) Tsang, W. Heats of Formation of Organic Free Radicals by Kinetic Methods. In *Energetics of Organic Free Radicals*; Martinho Simoes, J. A., Greenberg, A., Liebman, J. F., Eds.; Blackie Academic and Professional: London, 1996; pp 22.

(32) Wu, J. Y.; Liu, J. Y.; Li, Z. S.; Sun, C. C. *J. Chem. Phys.* **2003**, *118*, 10986.

(33) Galano, A.; Alvarez-ldaboy, J. R.; Ruiz-Santoyo, M. E.; Vivier-Bunge, A. *ChemPhysChem* **2004**, *5*, 1379.

(34) Chuang, Y. Y.; Corchado, J. C.; Truhlar, D. G. *J. Phys. Chem. A* **1999**, *103*, 1140.

CT800032E